Low-inductance capacitive probe for spark gap voltage measurements

David M. Barrett, Stanley R. Byron, Edward A. Crawford, Dennis H. Ford, Wayne D. Kimura, and Mark J. Kushner

Spectra Technology, Inc., 2755 Northrup Way, Bellevue, Washington 98004

(Received 8 April 1985; accepted for publication 15 July 1985)

A novel high-voltage (> 50 kV) capacitive probe has been developed to measure the voltage drop across a laser-triggered spark gap. The capacitors which comprise the voltage probe consist of three flat, annular rings that are housed within the spark gap chamber. The rings are oriented perpendicular to the spark column axis such that the column is formed in the open center of the rings. Polyethylene and Kapton foil are employed as dielectrics. The resistive portion of the divider is housed in a shielded enclosure external to the switch chamber. The inherent simplicity of the probe design ensures low inductance while minimizing stray capacitance; thus, the probe has excellent response characteristics ($\approx$ 1-ns theoretical rise time), and does not interfere with the performance of the switch. The probe has also been designed to permit access for laser triggering and interferometric measurements of the spark column formation. The voltage, current, and resistance characteristics of a laser-triggered spark gap for various gas mixtures are also discussed.

INTRODUCTION

Although spark gaps have been used as high-power switches in pulsed systems for many years, many processes which occur in these switches affecting their performance are still not well understood. Additionally, the parameters used to gauge the performance of a spark gap as a closing switch are not well described. One such parameter, switch loss, defined as the amount of energy which is deposited in the switch during the switching process, results from several factors, the principal one being gas heating due to the finite resistance of the arc channel. One may characterize the formation of an arc channel as having two distinct phases. During the first formative phase, current begins to flow while the arc resistance is still relatively high. As the arc continues to develop and expand, the channel resistance decreases until a small but finite value is reached. A small spark channel resistance is characteristic of the second phase often referred to as the conduction phase. Although resistive losses occur during both phases, these losses can be especially significant during the formative phase. Therefore, understanding of the arc formation is necessary in order to characterize the spark gap switch losses.

In order to gain a better understanding of the phases of spark gap arc development, Spectra Technology, Inc. has been characterizing a low impedance, laser preionized triggered spark gap. The experimental system, described elsewhere,[1] is shown in Fig. 1. The switch excitation source is a 1.5 Ω, 100-ns waterline which is pulse charged to voltages between 40 and 100 kV in 1.8 μs by a two-stage Marx bank. The spark gap consists of two hemispherical copper electrodes each having 1-mm-diam holes through their centers. The spark gap electrode spacing ranges from 1 to 2 cm. The preionization laser beam enters the switch through the hole in the anode and is focused to a point midway between the electrodes. The ionization channel thus formed produces a spark channel which is very reproducible, axisymmetric, and is accurately controllable both temporally and spatially. This permits the spark column to be studied using laser interferometric diagnostics. Access for optical diagnostics is provided by two sets of ports located orthogonally around the spark gap switch housing.

The impedance characteristics of the spark gap arc can be computed if the arc channel voltage and current are known. The arc current in this experiment is measured with a current viewing resistor (CVR). The CVR consists of an Inconel foil which serves as the current return path between the switch and the waterline. The arc voltage was initially measured with a resistive divider voltage probe originally developed at Los Alamos National Laboratory (LANL).[2] This probe was chosen because of its fast rise time and availability. However, the accuracy of the probe in this particular application suffered because of the method in which the probe was electrically connected to the spark gap. After consulting several sources,[3,4] it was decided that a capacitive voltage probe would give a more accurate indication of the switch voltage for our particular application. This paper describes the design and performance of a novel capacitive

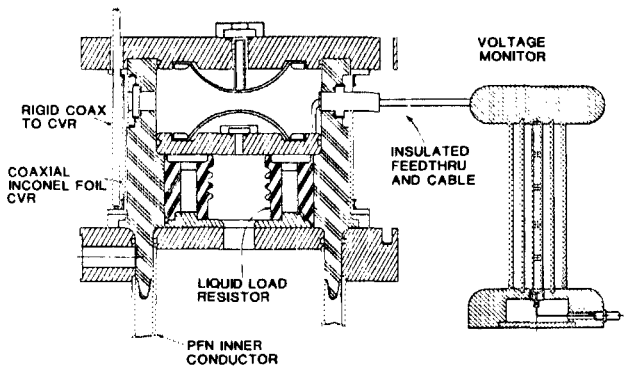

FIG. 1. Cross section of spark gap device illustrating the location of the voltage and current monitors.

 0034-6748/85/112111-05$01.30

probe used to characterize the arc channel of a laser-triggered spark gap.

I. DESCRIPTION OF THE CAPACITIVE VOLTAGE PROBE

The principal difficulty with applying the LANL resistive divider voltage probe to this experiment was related to the method in which the probe was connected across the spark gap. As shown in Fig. 1, the resistive probe was connected to the high voltage side of the spark gap with a section ($\approx$57 cm) of high-voltage wire. Charging the stray capacitance associated with the high-voltage terminal through this inductive lead caused spurious oscillations on the measured waveform. In designing an alternative to the resistive probe, it was desired to contain the major portion of the probe within the spark gap chamber thereby reducing the stray impedances and therefore minimizing the probe rise time.

In the initial design stages of the capacitive voltage probe, several configurations which employed discrete capacitors were considered; however, such designs were too large to be conveniently housed within the spark gap chamber and would therefore suffer from lead inductance problems also. The final design, shown in Fig. 2, incorporates the major portion of the probe within the chamber and uses a monolithic design for the two capacitors of the divider circuit.

An equivalent curcuit for the arc channel characterization experiment together with the capacitive probe is shown in Fig. 3. The PFL is charged to an initial voltage of V_s, the liquid load resistor is represented by R_L, and the inductance of the switch chamber is denoted by L_L. The spark channel is represented by a series resistance R_s and inductance L_s.

The output of the probe at time t can be expressed as

$$V_0(t) = \exp\left(\frac{-t}{RC}\right)\left[\frac{R_2 V_0(0)}{R} + \frac{R_2 C_1}{RC}\int_{t'=0}^{t'=t}\frac{dv_i(t')}{dt}\exp\left(\frac{t'}{RC}\right)dt'\right], \quad (1)$$

where $V_i(t)$ is the voltage across the spark gap, $C = C_1 + C_2$, and $R = R_1 + R_2$.

The capacitors, C_1 and C_2, consist of three, flat rings which are centered on the spark column axis and oriented

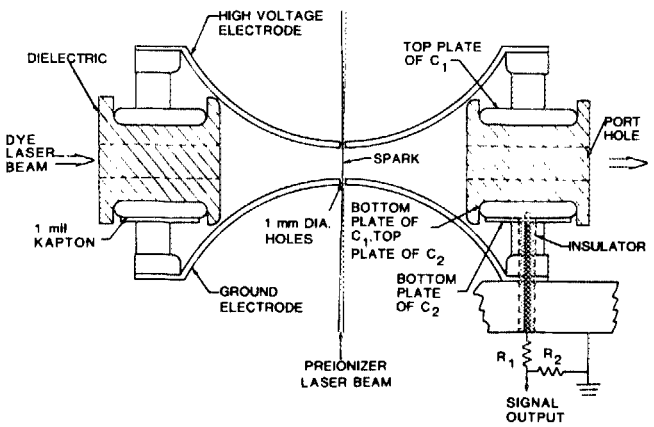

FIG. 2. Cross sectional view of the capacitive voltage probe installed inside the switch chamber.

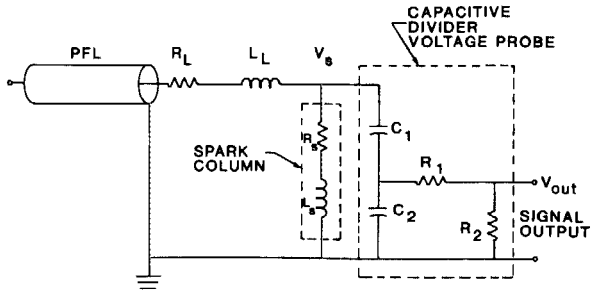

FIG. 3. Equivalent circuit for the switch chamber, spark column, and the capacitive voltage probe.

perpendicular to the axis (see Fig. 2). C_1 corresponds to the capacitance between top and middle rings while the capacitance between the middle and bottom rings is represented by C_2. The solid dielectric (polyethylene) interposed between the top and middle rings serves several useful purposes. It increases the capacitance of C_1 by approximately 2.3 times that for a gas dielectric and eliminates the possibility that the discharge will modify the dielectric properties of C_1. In addition, polyethylene has a higher dielectric strength than a gas and can be shaped to ensure a high voltage hold-off capability. Access for optical diagnostics which are used to examine the spark column is provided by holes drilled through the polyethylene annulus. Capacitor C_2 is constructed similarly to C_1; however, the dielectric for C_2 is a single layer of 0.025-mm-thick Kapton.

The electrical connection to the capacitors is made with a feedthrough which penetrates the end flange of the spark gap chamber and travels through one of the stand offs that support C_2. This configuration for the connection provides electrical shielding and eliminates dB/dt pickup. The resistive portion of the divider resides in a small shielded enclosure outside the spark chamber. With this arrangement, the voltage division ratio of the divider can be easily changed without switch disassembly by adjusting the values of R_1 and R_2.

The capacitance C_2 was easily determined to be 5 nF by using a vector impedance bridge. Because of the location of the electrodes of capacitor C_1, measurement is more difficult; however, its capacitance can be obtained by measuring the total attenuation of the probe for a known voltage input, and using the known values of R_1, R_2, and C_2 to calculate C_1. The voltage across the spark gap before breakdown is known from the resistive divider probe which is capable of accurately measuring the relatively slow (1.8 μs) pulse charging of the pulse forming line (PFL). The experimentally determined value of C_1 is 11.5 pF. This value agrees well with the geometrically calculated value of C_1.

As an additional check of the capacitance values, the decay time constant of the capacitive probe output can be measured. Since R_1 and R_2 are accurately known, and the attenuation factor is known, the values of C_1 and C_2 can be obtained from Eq. (1). Using this method, C_1 and C_2 are found to be 10.66 pF and 4.35 nF, respectively, which agrees well with the other determinations.

For conditions where the time scale of interest is short compared to RC, Eq. (1) may be rewritten as

$$V_0(t) = V_i(t)\,\alpha \exp(-t/\tau), \tag{2}$$

where α = attenuation factor = R_2C_1/RC and τ = probe time constant = RC. It can be seen from Eq. (2) that the time constant of the probe must be as long as possible to minimize the droop in the output signal. This fact implies large values of R_1 and C_2; however, since typically $C_2 \gg C_1$ and $R_1 \gg R_2$, the attenuation factor of the probe increases almost proportionately with values of R_1 and C_2. Therefore, their maximum values are subject to limits which will maintain an acceptable signal-to-noise ratio. Often in a practical design of a capacitive probe, the values of C_1 and C_2 are fixed, as in our design, and cannot be easily changed. Therefore, considerations of the attenuation ratio, probe time constant, and the signal-to-noise ratio often determine the value of R_1 alone. It is possible to choose the value of R_1 based on the amount of droop which can be tolerated during the voltage measurement. The e-fold error may be expressed as

$$\epsilon = [1 - \exp(\tau_p/R_1C_2)], \tag{3}$$

where τ_p is the pulsewidth of the voltage waveform to be measured. For this experiment, it was desired to measure the spark gap voltage from the beginning of the voltage collapse through the end of the conduction phase. The voltage waveform of interest has a width of approximately 100 ns. Resistors R_1 and R_2 are 2200 and 25 Ω, respectively. R_2 is actually a 50-Ω resistor in parallel with a 50-Ω cable impedance, terminated at the other end with 50 Ω. With the chosen values of R_1 and R_2, and the measured values of C_1 and C_2, the attenuation factor is 2.4×10^{-5}. This gives a time constant for the probe of 11.0 μs and an e-fold error (droop) of $< 1.0\%$ over an interval of 100 ns.

II. PERFORMANCE OF THE CAPACITIVE VOLTAGE PROBE

A comparison of the performance of the capacitive probe and the LANL resistive probe is shown in Fig. 4. In both Fig. 4(a) and 4(b) the upper trace is the output of the capacitive probe while the output of the resistive probe is the lower trace. The switch gas is SF_6, and the waterline is charged to $V_c \approx 40$ kV ($V_c/V_{SB(dc)} = 0.33$. Where $V_{SB(dc)}$ is the measured dc self-break voltage).

The waveforms for the two probes are very similar. Because the charging time of the waterline is 1.8 μs, which is a significant portion of the capacitive probe's time constant, the output signal of the probe when breakdown occurs corresponds to a voltage less than the charging voltage of the line. For our conditions, $V_0(0) = 0.91V_c$. When breakdown occurs, a signal which is proportional to the switch voltage appears at the output of the probe. Since voltage collapse occurs over a short time interval ($\leqslant 100$ ns) compared to the probe time constant, the output voltage does not suffer significantly from the droop and has an error of $< 1\%$. Due to the droop experienced during charging, the capacitive probe output voltage crosses zero and slowly decays with the time constant of the probe. The true zero of the capacitive probe is indicated on Fig. 4.

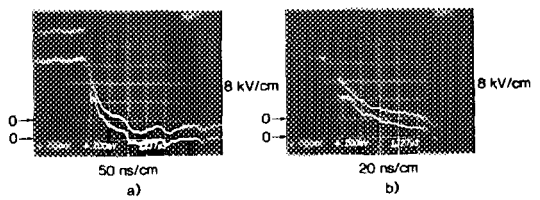

FIG. 4. Resistive probe (lower waveform in each trace) and capacitive probe (upper waveform in each trace) output waveforms when the switch chamber is filled with 100% SF_6. The upper zero in each case indicates the base line for the capacitive voltage probe while the lower zero indicates the base line for the resistive probe.

If one compares the waveforms for the capacitive and resistive probe, the effects of the stray capacitance on the resistive voltage divider are clearly evident. Fast transitions in the spark gap voltage (i.e., voltage collapse during breakdown) result in oscillations (i.e., ringing) which are present on the output signal of the resistive divider. Eventually, these oscillations are damped such that the output waveform of the resistive probe is in good agreement with the waveform of the capacitive probe.

The rise time of the capacitive probe may be estimated by calculating the inductance of the cavity which is formed by the electrode structure with the probe. The cavity inductance and the probe capacitance define a resonant frequency which is indicative of the probe's rise time. This method yields an estimated rise time for the probe of ≈ 1 ns.

The fast response time of the capacitive probe is demonstrated experimentally in Fig. 5. This shows the voltage waveforms measured by the capacitive probe and the resistive probe for a 1% Xe/99% H_2 gas mixture at 2 at. absolute and with the waterline charged to $V_c \approx 38$ kV ($V_c/V_{SB(dc)} = 0.95$). The resistive probe output (lower trace) displays definite ringing immediately after voltage collapse. The capacitive probe output (upper trace) does not display these gross oscillations; however, it does have high-frequency oscillations (≈ 300 MHz) immediately after voltage collapse and again 100 ns later (corresponding to the peak of the current pulse). We believe these high-frequency oscillations originate from the spark column dynamics. The reasons are as follows: First, the voltage changes only moderately at 100 ns after breakdown; indeed, the resistive probe follows the voltage accurately at this point without ringing. Second, the presence of the high-frequency oscillations are a function of the average molecular weight of the switch gas mixture. In Fig. 4, for the case of 100% SF_6, the high-frequency oscillations are absent. As will be shown later in Fig. 6, the oscillations become more evident as the average molecular weight of the gas mixture decreases. Additionally, a computer model,[5] developed to model the spark column formation, predicts oscillations which are driven by the dynamics of the

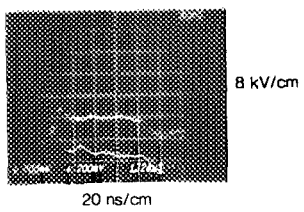

FIG. 5. Resistive probe (lower waveform) and capacitive probe (upper waveform) output waveforms when the switch chamber is filled with 1% Xe/99% H_2.

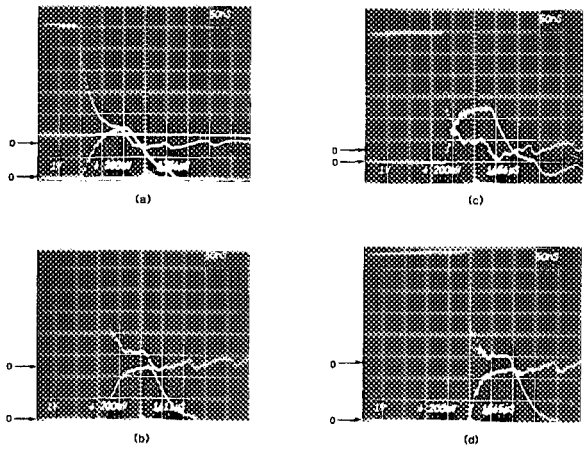

FIG. 6. I-V waveforms for 2 at., 40-kV experiments in different gas mixtures: (a) 100% SF_6, (b) 5% SF_6/20% N_2/75% He, (c) 20% CH_4/80% H_2 (d) 1% Xe/99% H_2.

spark column itself at the same frequency as observed for this gas mixture.

III. SPARK GAP VOLTAGE AND CURRENT DATA

The capacitive probe was used to measure the voltage drop across a laser-triggered spark gap switch. Simultaneous current measurements were used to calculate the impedance of the arc channel. In addition, concurrent interferograms of the spark channel were taken. These interferograms yielded values for the diameter of the spark column. The channel inductance was estimated from these values and the resistance of the channel was then inferred from the impedance measurements.

Voltage and current waveforms for different laser-triggered gas mixtures are shown in Fig. 6. In all cases, the switch pressure is 2 at. absolute, the waterline was charged to approximately 40 kV. Figure 6(a) is for a 100% SF_6 gas mixture; Fig. 6(b) for a 5% SF_6/20% N_2/75% He mixture; Fig. 6(c) for a 20% CH_4/80% H_2 mixture; and Fig. 6(d) for a 1% Xe/99% H_2 gas mixture. The average molecular weight of each mixture is 146, 15.9, 4.8, and 3.3 AMU, respectively. A number of qualitative observations can be made. Both the voltage fall time and the conduction phase voltage decrease with decreasing average molecular weight; the rate rise of current increases with decreasing average molecular weight. Also note that the peak spark gap current is not a function of the gas mixture.

These observations imply that the resistance of the spark column is, to first order, a monotonic function of the average molecular weight of the switch gas. These observations are consistent with the view that the dominant growth mechanism for the spark channel is a hydrodynamic expansion of the hot ionized gas. Therefore, for a switch whose operation requires low losses and fast switching times, a low molecular weight gas should be used. The reduced jitter and improved voltage hold off (i.e., operating at low percentages of self-break) obtained with laser triggering enables the use of light gases.

It is possible to determine the true resistance and conductivity of the spark channel from the voltage and current waveforms. The task though is complicated by an inductive component which is present in the measured spark channel voltage. Therefore, it is necessary to determine and subtract the inductive component from the measured waveform. The capacitive voltage probe measures the quantity

$$V_s = I(t)R_s(t) + [L_s(t) + L_f]\frac{dI(t)}{dt} + I(t)\frac{dL_s(t)}{dt}, \quad (4)$$

where L_f is a constant value based on the geometry. For our experimental conditions, the last term in Eq. (4) is small and can be neglected. The voltage and current waveforms from Fig. 6. were digitized and entered as inputs to a computer program which solves Eq. (4). Numerical differentiation of the current waveform provides $dI(t)/dt$. The last remaining quantity required to solve for $R_S(t)$ is the spark channel inductance $L_s(t)$. This value is obtained from the time history of the spark channel radius as indicated by the interferograms taken coincidentally with the voltage and current measurements. Assuming current flows uniformly through the spark column, the value of $L_s(t)$ is given approximately by

$$L_s(t) \cong l(\mu_0/2\pi)\ln[r_c/r_s(t)], \quad (5)$$

where l is the length of the spark column, r_c is the radius of the current return path, and $r_s(t)$ is the radius of the spark channel given by the interferograms. With the value of $L_s(t)$, it is now possible to solve for the spark channel resistance $R_s(t)$.

The resistances of the spark channel calculated in this manner for the gas mixtures given in Fig. 6 are plotted in Fig. 7. The data confirm the conclusions drawn from the qualitative observations made from the I-V characteristics of the spark column: the resistance of spark channel decreases with average molecular weight of the insulating gas.

IV. DISCUSSION

Although capacitive voltage divider probes are generally known devices, their usage and specific designs are usually very dependent on the geometry of the experimental system. This is because one or both of the capacitors which comprise the capacitive voltage divider circuit are usually the capacitance between parts of the experimental system and the probe. For example, in the case of sensing a voltage along a

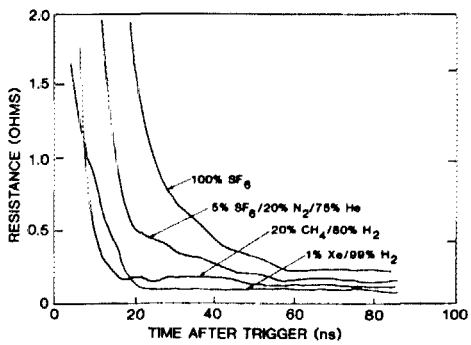

FIG. 7. Spark column resistance obtained by computer processing of experimental I-V traces.

waterline, the capacitor referred to as C_1 in Fig. 3 is typically the capacitance between the inner conductor of the waterline and the probe; and capacitor C_2 is the capacitance between the outer conductor of the waterline and the probe.

Our design, however, is not highly dependent on the experimental geometry. The design philosophy we have adopted of creating the two capacitors physically separate and independent of the experimental system frees us from being limited by the geometry of the system. This in fact permitted our probe to have a very fast response time because it could be designed for low inductance. In addition, the capacitors can be positioned directly across the voltage potential of interest. Hence, we are able to measure the voltage directly across the spark gap and are not forced to measure it across, say, the spark gap and the load resistor in series.

Taking this design freedom a step further: Had the geometry of our spark gap chamber been rectangular, the probe could have been designed with a rectangular cross section with no significant loss in performance. The geometrical flexibility inherent to this design makes it a candidate for many other applications such as coaxial or rectangular electron-beam diodes.

Another noteworthy point of our probe is that its calibration is straightforward. By following the steps given in this paper, where we have been careful to include all contributions to the probe response, other probes based upon general design principles of the one described can be accurately calibrated.

ACKNOWLEDGMENTS

The authors wish to aknowledge the assistance of J. F. Seamans in the setup of the optical diagnostic system. This work was supported by the Naval Surface Weapons Center, Contract No N60921-83-C-A057.

[1]W. D. Kimura, E. A. Crawford, M. J. Kushner, and S. R. Byron, in *Proceedings of the 16th IEEE Power Modulator Symposium* (IEEE, Arlington, VA, 1984), p. 54.
[2]W. L. Willis, Los Alamos National Laboratory, Report No. LAUR-80-2272, 1980.
[3]D. B. Fenneman, Naval Surface Weapons Center, Dahlgren, VA (private communication).
[4]A. J. Schwab, *High Voltage Measurements Techniques* (MIT, Cambridge, 1972), p. 65.
[5]M. J. Kushner, R. D. Milroy, and W. D. Kimura, J. Appl. Phys. **58**, 2988 (1985).